Balancing stiffness and ductility in starch–lignin bioplastics using binary and ternary deep eutectic solvents (ChCl:Gly:MEA)

Phuong Thi Hoang*, Chien Nguyen Van, Phuong Ha Doan, Trang Quynh Pham

Institute of Chemistry, Vietnam Academy of Science and Technology

18 Hoang Quoc Viet, Nghia Do Ward, Hanoi, Vietnam

Received 8 October 2025; revised 16 October 2025; accepted 16 November 2025

Abstract

Deep eutectic solvents (DESs) offer a green route to tailor starch–based plastics, yet how composition controls the interphase and aging in corn starch-lignin (CS–Lig) matrices remains unclear. Binary and ternary DESs were prepared from choline chloride (ChCl), glycerol (Gly), and monoethanolamine (MEA). In this study, CS–Lig was melt-processed with Gly (control) or with binary (ChCl:Gly 1:3; ChCl:MEA 1:3) and ternary ChCl:Gly:MEA DESs (1:1:1; 1:1:2; 1:2:1). We combined dynamic mechanical analysis (DMA), tensile testing, Fourier transform infrared (FTIR), X-ray diffraction (XRD), scanning electron microscopy (SEM), and Owens–Wendt–Rabel–Kaelble (OWRK) wettability; we also integrated 0–56-day retrogradation assays. Relative to glycerol, DESs systematically enhanced performance: tensile strength (TS) rose to ≈ 2.97 MPa (CS–Lig–C.G.M 1:2:1) and elongation (ε_b) to ≈ 184 % (CS–Lig–C.G.M 1:1:2). One-way ANOVA ($p < 0.001$) and Tukey HSD separated ternary DESs from the control. FTIR showed broadened, red-shifted –OH/–NH envelopes; XRD indicated reinforced V-type order; SEM revealed tighter lignin encapsulation. Surface polarity was tuneable ($\gamma \approx 41–58$ mN m^{-1}), and specific DESs mitigated aging-related losses. This composition–property map provides practical design rules to target strength/stiffness (e.g., 1:2:1) or ductility (e.g., 1:1:2) in greener CS–Lig bioplastics.

Keywords: **bioplastics, choline chloride–glycerol–monoethanolamine, corn starch–lignin blend, deep eutectic solvent.**

Classification number: **2.2**

1. Introduction

*Corresponding author: Email: hoangphuong15@gmail.com

Biobased CS–Lig blends are attractive for replacing petroleum plastics in packaging owing to renewability and end-of-life advantages, yet they remain limited by moisture sensitivity, brittleness, and time-dependent retrogradation that degrades ductility and processability. Blending starch with lignin can reinforce networks and improve water resistance but does not by itself resolve the stiffness–ductility trade-off or long-term aging [1, 2]. A central lever is plasticisation: conventional polyols such as Gly lower the glass transition and facilitate melt processing, but may migrate, increase water uptake, and accelerate post-processing recrystallisation (retrogradation) [3, 4].

DESs have emerged as "designer" plasticisers/solvents formed by hydrogen-bond acceptor/donor pairs (e.g., ChCl with polyols or alkanolamines). Their appeal lies in tuneable polarity, strong and reversible H-bond/ion–dipole interactions with polysaccharides, and often benign sourcing. Recent reviews and case studies show that DESs can plasticise starch, modulate thermal–mechanical response, and, in some systems, mitigate aging; ternary DESs further expand the design space and have been explored with thermoplastic starch (TPS) and TPS/lignin matrices [5-7]. At the molecular level, spectroscopy and modelling indicate that ChCl-based DESs interact via predominant H-bonds between Cl^- (the hydrogen bond acceptor (HBA)) and –OH/–NH groups of polyols/alkanolamines (the hydrogen bond donor (HBD), offering a plausible handle to balance segmental mobility against network cohesion [8].

Beyond bulk mechanics, wettability and interfacial behaviour govern printing/lamination and barrier performance. Here, surface free energy (SFE) is resolved into dispersive and polar components using OWRK analysis from multi-liquid contact angles, an approach established for polymer surfaces and widely implemented in modern goniometry [9].

Despite these advances, a systematic mapping of binary versus ternary ChCl DESs containing Gly and MEA within a CS–Lig matrix, linking thermo-viscoelasticity (DMA), tensile testing (TS, ε_b), OWRK, and 0–56-day retrogradation, has not been comprehensively quantified. Building on the DES-TPS/TPS-lignin literature, we ask whether cooperative H-bond/ion–dipole networks in ChCl:Gly:MEA ternaries can alleviate the conventional plasticisation–stiffness trade-off while slowing retrogradation, relative to Gly and binary DES baselines [5, 7].

In this work, we engineer six CS-Lig formulations (Gly control; binary DESs rich in MEA or Gly; and three ternary ChCl:Gly:MEA ratios) and (i) quantify T_g and E′ by DMA, (ii) evaluate TS and ε_b at t = 0 and after storage (7/28/56 days), (iii) determine SFE components from contact angles with water, formamide, and diiodomethane, and (iv) apply inferential statistics (one-way ANOVA, Tukey HSD) to establish significance. We show that composition-guided DES design provides a tuneable path to concurrently lower T_g, maintain or raise small-strain stiffness, optimise strength–ductility balance, and reduce retrogradation penalties, outcomes directly relevant to scalable, greener CS–Lig bioplastics [3, 6].

Despite reports on TPS/DES blends, lignin-containing systems remain underexplored. In particular, how DES composition, ChCl:MEA, ChCl:Gly, and ChCl:Gly:MEA modulates interfacial hydrogen-bonding at the CS-Lig boundary, surface polarity/adhesion (OWRK), and property retention during storage has not been mapped systematically. Here we address this gap by systematically comparing binary (ChCl:MEA 1:3; ChCl:Gly 1:3) and ternary (ChCl:Gly:MEA 1:1:1, 1:1:2, 1:2:1) DESs in CS–Lig matrices, and by quantitatively linking FTIR-derived H-bond metrics with surface-energy and mechanical responses.

2. Materials and Methods

2.1. Chemicals

Glycerol (≥ 99.5 %), choline chloride (≥ 99.0 %), and monoethanolamine (≥ 99.0 %) were purchased from Merck and used as received. Binary and ternary DES were prepared at mole ratios ChCl:Gly 1:3, ChCl:MEA 1:3, ChCl:Gly:MEA 1:1:1, ChCl:Gly:MEA 1:1:2, and ChCl:Gly:MEA 1:2:1 by heating at 80–90°C with gentle stirring until clear (about 30 minutes to 2 hours depending on the DES), homogeneous liquids formed. Warm DESs were transferred to airtight containers and stored at ambient temperature. Corn starch (amylose 22–28 %, moisture ≈ 13 %, ash 0.2 %) was obtained from NEO Nam Vietnam. Lignin was isolated from Bai Bang Paper Mill kraft black liquor as described in Section 2.3.

2.2. Analytical methods

Tensile properties: Compression-moulded plaques were die-cut into ASTM D638 Type IV dumbbell specimens (gauge length 25 mm; neck width 6.00 ± 0.05 mm; thickness 3.00 ± 0.10 mm). Tests were performed on a 10 kN universal testing machine at a crosshead

speed of 20 mm/min at ambient conditions. Tensile strength (TS) and elongation at break (ε_b) were extracted from engineering stress–strain curves, following ASTM D638 using an AGX-V Testing Machine (Japan). Values were averaged over five specimens (n = 5).

X-ray diffraction: Diffractograms were collected on a Bruker D8 ADVANCE (Germany) with Cu Kα radiation (λ = 0.154 nm) at 40 kV/30 mA, scanning 2θ = 10–70° at 2°/min (step 0.02°).

Dynamic Mechanical Analysis: Bars machined from plaques were tested on a DMA1 (Mettler Toledo, Switzerland) in single-cantilever mode from -40 to 120°C at 10 °C/min, 1 Hz, within the linear viscoelastic regime (0.1 % strain) verified by a preliminary strain-sweep. The glass-transition temperature (T_g) was taken at the tan δ maximum; storage modulus (E') was recorded over the same temperature range (n = 3).

FTIR spectroscopy: Spectra were recorded on a NicoletTM iS50 (ATR mode, diamond) over 4000–500 cm^{-1} at 4 cm^{-1} resolutions and 16 scans per spectrum. The OH/NH envelope (3800–3000 cm^{-1}) was assessed using two quantitative descriptors extracted from the already-acquired ATR spectra: (i) the OH red-shift (ΔνOH) of the band maximum/centroid relative to the Gly control, and (ii) the full-width at half-maximum (FWHM) of the envelope. For completeness, we refer to a conventional hydrogen-bond index (HBI), defined as A(3200–3400)/A(3570–3600), as an interpretive proxy of strongly H-bonded populations. No additional experiments or figures were generated; these descriptors are used to interpret the trends visible in the reported spectra.

Morphology: Scanning electron microscopy (SEM, SM-6510LV (JEOL, Japan) at the Institute for Tropical Technology. Samples were fractured in liquid nitrogen and sputter-coated with a thin platinum layer.

Surface wetting properties: Static contact angles (water, formamide, diiodomethane) were measured (DSA25, KRÜSS) at 25 ± 2°C. For each liquid, three drops (5 µL) were placed on three distinct regions (n = 3 per liquid). Total SFE (γ) and its dispersive (γ^d) and polar (γ^p) components were obtained by OWRK using KRÜSS ADVANCE. Units are reported in mN m^{-1}. $f_p=\gamma^p/\gamma$, $W_{sl}=\gamma_{lv}(1+\cos\theta_{H2O})$ and $W_{12}=2(\sqrt{\gamma_{1d}\,\gamma_{2d}}+\sqrt{\gamma_{1p}\,\gamma_{2p}})$ following the Owens–Wendt–Kaelble framework [9]. Liquid surface tensions at 20–25°C were taken as: water 72.8 (γ^d = 21.8, γ^p = 51.0) mN m^{-1} [10]. Reference substrate components (mN m^{-1}) were cellulose (γ^d = 29.0, γ^p = 16.0) [11].

Aging protocol: After initial testing (day 0), specimens were stored in a controlled chamber at 23 ± 2 °C, 50 ± 5 % RH and retrieved at 7, 28, and 56 days for tensile re-evaluation under identical conditions. Each timepoint included re-conditioning per ASTM D618 and ISO 291. Aging analysis focused on retention of TS and ε_b relative to day 0 (n = 5). Mechanical retention at 7/28/56 days (23°C/50 %RH) is used as the functional surrogate of retrogradation-driven microstructural change in TPS.

Data analysis: R programming was used for statistical analysis of the obtained results. All data are presented as mean ± standard deviation (SD). Each experiment was repeated in triplicate (n = 3 / n = 5) and statistical analysis was conducted using one-way ANOVA followed by Tukey's HSD test, with $p < 0.05$ considered significant. Compact letter displays (a, b, c) denote homogeneous groups; values sharing a letter are not significantly different.

2.3. Isolation of lignin from Kraft black liquor

Black liquor was concentrated to ≈ 35 wt% total solids at 70°C by rotary evaporation, then acidified to pH 2.0–2.5 with 98 % H_2SO_4 under stirring at 55 ± 2°C. After 45 min, the precipitated lignin was collected by vacuum filtration, rinsed with pH ≈ 2 water, air-dried, and then vacuum-dried at 50°C to constant mass. Low-molecular-weight fractions were reduced following Saito et al., 2014 [12] with modifications: ethanol washing at a 1:7 (m/v) lignin:ethanol ratio, sonication at 30°C, centrifugation (8000 rpm, 15 min), repeated four times, then oven- and vacuum-drying at ≈ 50°C. The final lignin showed $M_n = 4.68 \times 10^3$ g mol^{-1}, $M_w = 1.12 \times 10^4$ g mol^{-1}, PDI = 2.39, and ash 0.67 wt%.

2.4. Preparation of CS–Lig–DES polymer blend samples

Corn starch was oven-dried (60°C, 8 h) and equilibrated in a desiccator. All CS–Lig formulations used a fixed plasticiser loading of 20 g (total-mass basis); plasticiser identity and DES molar ratios followed Table 1. To minimise feed variability, dried starch and plasticiser were pre-homogenised at room temperature in a sealed batch mixer to a free-flowing moist premix, then immediately fed to the extruder. This step was applied uniformly to Gly and all DES systems. Compounding was carried out on a co-rotating twin-screw extruder (HAAKE Rheomex PTW16/25 OS, Thermo Scientific; D = 16 mm; L/D ≈ 25). The barrel profile was 110 °C (feed), 120–125°C (melting), 115–120°C (mixing/conveying), and 110°C (die); screw speed 150 rpm. Strands were air-cooled, pelletised, and conditioned for 24 h at 23 ± 2°C and 50 ± 5% RH. Pellets were

compression-moulded at 120°C into plaques 3.00 ± 0.10 mm thick under ~4.4 MPa for 3 min, then cooled to ~60°C before demoulding. Unless otherwise specified, specimens were conditioned at 23 ± 2°C and 50 ± 5% RH for ≥40 h before characterisation. Formulation codes and compositions are given in Table 1.

Table 1. Formulations of CS–Lig blends plasticised with Gly or DES

Samples	Composition (g)			Plasticiser type	DES Ratio		
	Corn starch	*Lignin*	*Plasticiser*		*ChCl*	*Gly*	*MEA*
CS–Lig–Gly	50	10	20	Gly	-	-	-
CS–Lig–C.M 1:3	50	10	20	DES	1	-	3
CS–Lig–C.G 1:3	50	10	20	DES	1	3	-
CS–Lig–C.G.M 1:1:1	50	10	20	DES	1	1	1
CS–Lig–C.G.M 1:1:2	50	10	20	DES	1	1	2
CS–Lig–C.G.M 1:2:1	50	10	20	DES	1	2	1

3. Results and Discussion

3.1. Thermo-Viscoelastic Behaviour by Dynamic Mechanical Analysis (DMA)

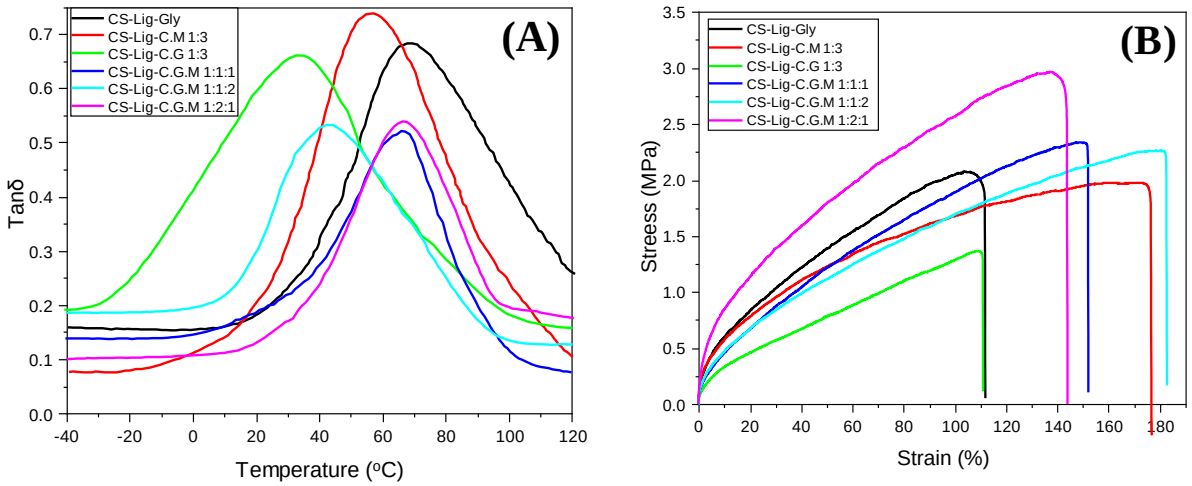

Fig. 1. Thermo-mechanical properties of CS–Lig–plasticiser samples: (A) tan δ–temperature curves (n = 3); (B) tensile stress–strain curves (mean ± SD, n = 5).

Table 2. Summary of thermal–viscoelastic properties (T_g, E', mean ± SD, n = 3) and mechanical results (mean ± SD, n = 5) of CS–Lig–plasticiser samples.

Samples	Thermal – viscoelastic properties		Mechanical properties		
	T_g, °C	*E'_{max}, MPa*	*TS (MPa)*	*ε_b (%)*	*ε_b (CV%)*
CS–Lig–Gly	68.6 ± 4.9[a]	967.8 ± 69.7[a]	1.14 ± 0.07[d]	109.7 ± 12.3[c]	11.2

CS–Lig–C.M 1:3	56.1 ± 3.3^{b}	820.7 ± 68.9^{ab}	1.97 ± 0.14^{c}	176.9 ± 18.8^{ab}	10.6
CS–Lig–C.G 1:3	33.9 ± 2.4^{c}	578.3 ± 53.2^{c}	1.36 ± 0.11^{d}	111.3 ± 13.4^{c}	12.0
CS–Lig–C.G.M 1:1:1	65.2 ± 5.4^{a,b}	764.2 ± 58.1^{b}	2.34 ± 0.22^{b}	152.4 ± 14.8^{ab}	9.7
CS–Lig–C.G.M 1:1:2	42.7 ± 2.2^{c}	922.4 ± 65.5^{a}	2.26 ± 0.14^{bc}	184.2 ± 15.8^{a}	8.6
CS–Lig–C.G.M 1:2:1	66.8 ± 3.3^{a}	936.1 ± 76.8^{a}	2.97 ± 0.18^{a}	148.6 ± 15.3^{b}	10.3

Note: Coefficient of variation (CV%) is reported for εb to normalise dispersion at high ductility. Superscripts (a, b, c) denote homogeneous groups from Tukey's HSD (α = 0.05).

T_g was taken from the tan δ maximum (Fig. 1A). The glassy-region stiffness was characterised by E'_{max}. The control (CS–Lig–Gly) shows $T_g \approx 68.6$°C and $E'_{max} \approx 968$ MPa, reflecting a dense H-bonded network where Gly affords only moderate plasticisation. CS–Lig–C.M 1:3 (MEA-rich) lowers T_g by ≈ 12.5°C with a moderate drop in E'_{maC}, consistent with increased free volume coupled to H-bond/ion–dipole interactions [6]. In the MEA-rich binary DES (CS–Lig–C.M 1:3), plasticisation is moderated: T_g decreases by 12.5°C relative to the control (from 68.6°C to 56.1°C), accompanied by a reduction in. This behaviour suggests that MEA, rich in –NH/–OH groups, increases free volume while simultaneously forming hydrogen-bond/ion–dipole interactions with CS/Lig, thereby improving ductility yet maintaining a comparatively high modulus [7, 13, 14]. By contrast, the Gly-rich binary DES (CS–Lig–C.G 1:3) exhibits marked plasticisation: both T_g and E'_{max} drop substantially versus the control ($\Delta T_g = -34.7$°C , $\Delta E'_{max} = -389.5$ MPa), consistent with increased starch-chain mobility in Gly-rich DES [6, 15]. Ternary DESs indicate cooperative interactions among constituents and overall reductions relative to the control. CS–Lig–C.G.M 1:1:1 yields $T_g \approx 65.2$°C (near the control) and $E'_{max} \approx 764.2$ MPa, suggesting a balance whereby Gly enhances segmental mobility while MEA provides hydrogen-bond/ion–dipole interactions that partially immobilise the plasticiser [7, 13, 14]. The Gly-rich ternary DES (CS–Lig–C.G.M 1:1:2) has a lower $T_g \approx 42.7$°C while maintaining a high $E'_{max} \approx 922.4$ MPa, implying synergistic effects: MEA-mediated interactions help sustain stiffness as Gly increases free volume [7, 13, 14]. Upon further increasing Gly (CS–Lig–C.G.M 1:2:1), $T_g \approx 66.8$°C (close to the control) while $E'_{max} \approx$ 936.1 MPa, which may reflect a high density of hydrogen-bond/ion–dipole interactions that constrains plasticisation [7, 13, 14].

One-way ANOVA (Table S1) confirms large between formulation effects for both metrics: T_g (F = 43.21, p = 2.90 ×10^{-7}, E′ (F = 14.75, p = 1.0 ×10^{-4}. These statistics indicate that formulation explains the majority of variance in the thermo-viscoelastic response. Tukey's HSD (Table S2) locates the principal pairwise differences for T_g (CS–Lig–C.G 1:3) vs CS–Lig–Gly (Δ = −34.7°C; adjusted $p \approx 0$), CS–Lig–C.G.M 1:1:2 vs CS–Lig–Gly (Δ = −25.9°C; $p \approx 0$), and CS–Lig–C.G 1:3 vs CS–Lig–C.M 1:3 (Δ = −22.2°C; p = 10^{-4}); CS–Lig–C.G.M 1:2:1 vs CS–Lig–C.M 1:3 is moderately higher in T_g (Δ = +10.7°C; p = 0.041). These pairwise outcomes are consistent with the ranking in Table 2 and with the qualitative trends in Fig. 1A.

3.2. Mechanical properties

Figure 1B and Table 2 summarise the tensile behaviour (mean ± SD, n = 5). Although the absolute SD of ε_b appears larger for the most ductile formulations, the normalised dispersion remains modest (CV ≈ 8.6–12.0%), and one-way ANOVA with Tukey's HSD still separates the groups clearly, preserving the inference on formulation effects. Relative to the Gly control CS–Lig–Gly (TS = 1.14 ± 0.07 MPa; ε_b = 109.7 ± 12.3 %), all DES-plasticised blends display clear improvements in strength and ductility. The MEA-rich binary CS–Lig–C.M 1:3 attains TS = 1.97 ± 0.14 MPa and ε_b = 176.9 ± 18.8 %, indicating a substantial, simultaneous gain in both metrics. By contrast, the Gly-rich binary CS–Lig–C.G 1:3 shows only a modest strength increase (TS = 1.36 ± 0.11 MPa) with essentially unchanged ductility (ε_b = 111.3 ± 13.4 %). Among the ternaries, CS–Lig–C.G.M 1:1:1 achieves a balanced response (TS = 2.34 ± 0.22 MPa; ε_b = 152.4 ± 14.8 %), whereas CS–Lig–C.G.M 1:1:2 maximises ductility (ε_b = 184.2 ± 15.8 %) at high strength (TS = 2.26 ± 0.14 MPa). The highest strength is delivered by CS–Lig–C.G.M 1:2:1 (TS = 2.97 ± 0.18 MPa) with still-high elongation (ε_b = 148.6 ± 15.3 %). Taken together, the ternary systems provide the best strength–ductility balance, while the MEA-rich binary outperforms the Gly-rich binary. This is explained by the fact that, in the Gly-rich system, the trend of increasing TS and ε_b is not high because the excess Gly causes plasticisation of the starch matrix (significantly reduces T_g) but does not create strong enough interphase bonds with lignin, leading to poor stress transmission [6, 15]. In the MEA-rich system, both TS and ε_b increase sharply, possibly due to the H-bond/ion–dipole interphase interactions between the –NH/–OH groups of MEA and the -OH groups of CS and phenolic groups of lignin, both increasing the mobility of the molecular chain (increased ε_b) and

improving the ability to transmit stress (increased TS). With the three-component DES system, the highest increase in TS was recorded in the 1:2:1 system while the increase in ε_b was shown in the 1:1:2 system. This is due to the balance between the interaction of Gly providing the mobility of the matrix polymer and MEA promoting the interphase interactions between the plasticiser with CS and lignin [7, 13]. In addition, the role of lignin can strengthen the CS matrix through H-bond interactions at the interfacial interface; when combined with DES (especially the ternary system), the compatibility and dispersibility of lignin in the matrix increase, thereby improving TS without significantly reducing ε_b. Thereby, in the 1:1:2 sample, T_g is significantly reduced but E′ remains high while ε_b increases sharply. Recent studies also show that the multi-point H-bond network formed in the blend system (CS –DES –Lig) is the key to enhancing stress transmission and reducing interfacial defects [16, 17].

One-way ANOVA (Table S1) confirms a pronounced formulation effect for both TS and ε_b ($F = 99.65$; $p = 3.014 \times 10^{-15}$ and $F = 21.51$; $p = 3.743 \times 10^{-8}$, respectively), with large effect sizes (partial $\eta^2 \approx 0.90–0.95$ for TS; $\approx 0.75–0.90$ for ε_b). Tukey's HSD (Table S4) localises the differences: versus the control, all MEA-containing DESs yield significant strength gains (e.g., +1.20 to +1.83 MPa, adjusted $p \ll 0.001$), whereas CS–Lig–C.G 1:3 is not different in TS (adjusted $p = 0.2315$). For ductility, CS–Lig–C.G.M 1:1:2 exhibits the largest improvement (+74.5 percentage points; adjusted $p \approx 0$), followed by CS–Lig–C.G.M 1:1:1 and CS–Lig–C.G.M 1:2:1, while CS–Lig–C.G 1:3 remains statistically unchanged. These statistical outcomes mirror the rank ordering visible in Figure 1B and the summary in Table 2.

3.3. FTIR spectrum

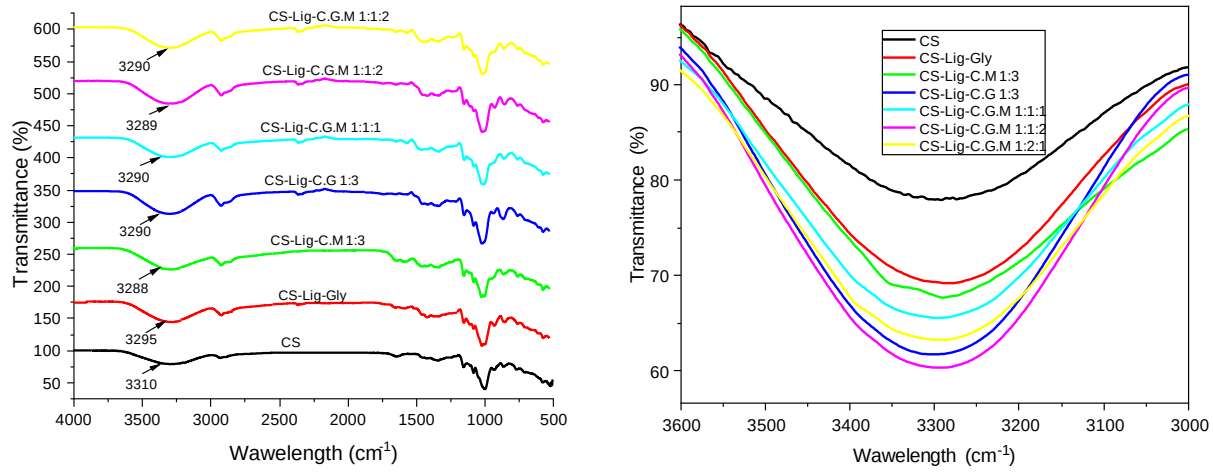

Fig. 2. FTIR spectra of CS and CS–Lig samples plasticised with different DES systems

Results Figure 2 shows that the FTIR spectra of the samples show characteristic absorption bands in the region of 3600–3000 cm^{-1} which are characteristic vibrations of the –OH group and the overlap of –OH/-NH in the samples containing MEA. Compared with the control sample (CS–Lig–Gly), the spectra of the samples plasticised with DES show a wider absorption band of –OH and a tendency to shift to low wavenumber (red-shift) at different levels between the formulas. This is due to the density of H-bonds between DES-CS-Lig (–OH of starch/phenolic-OH of lignin with –OH/–NH of DES), reflecting the state of both plasticisation and interphase H interaction instead of just plasticisation like traditional Gly [7, 13]. The stretching vibration of the C–H bond is shown in the region of 2930/2850 cm^{-1} with the same intensity between the formulas. The polysaccharide backbone (characteristic of C–O/C–O–C bonds in the absorption peak region 1200–900 cm^{-1}) showed changes in shape and intensity in this band between the control and DES samples, indicating the modification of the intramolecular hydrogen bonding network with DES. Lignin features include: aromatic ring vibrations at 1600–1510 cm^{-1}; phenolic C–O bonds at 1260–1210 cm^{-1}) [18, 19]. These bands were present and varied relatively between the formulations, supporting the notion that DES improved interphase compatibility (CS-Lig) through multipoint H-bonding, especially when MEA (containing both –NH/–OH) and Gly (rich in –OH groups) were present in the ternary DES system. The DES ChCl-Gly system has a multi-H-bond network, increasing the ability to interact with the phenolic –OH group of lignin and –OH of starch. On the TPS/DES/Lignin (ternary) system, FTIR and properties show increased compatibility at the interfacial surface; amine-DES (containing –NH, like MEA) alone adds a H-bond donor–acceptor centre, contributing to the absorption intensity in the –OH/–NH region [7, 17, 19, 20].

Relative to the Gly-rich binary, MEA-containing DESs display a clearer low-frequency growth and broadening of the OH/NH envelope (consistent with larger Δν_OH and FWHM), indicating a denser and more broadly distributed H-bond network. This spectroscopic signature coheres with the higher storage modulus in DMA and the reinforced V-type ordering in XRD, thus supporting our 'multi-site hydrogen-bonding' interpretation without requiring additional experiments.

3.4. X-Ray Diffraction (XRD) Patterns

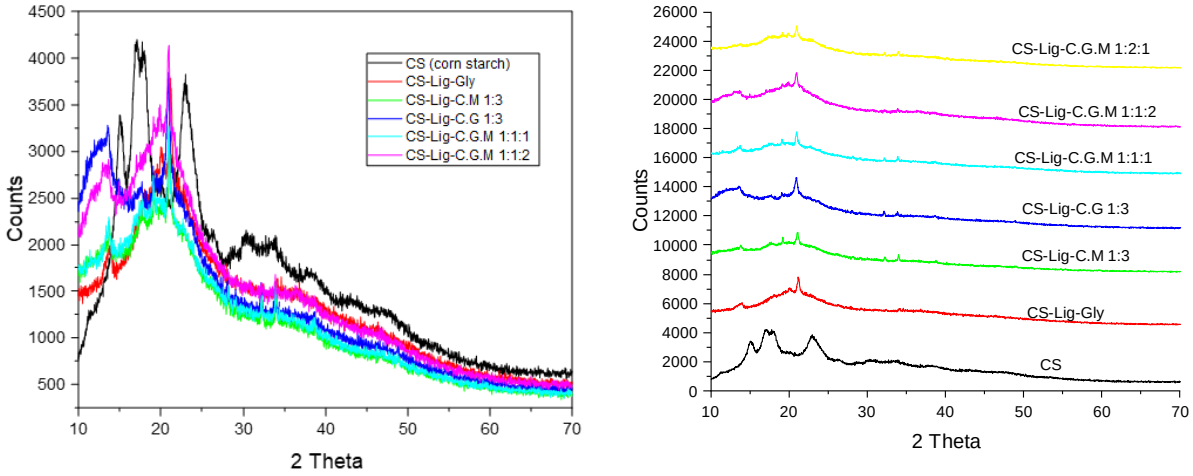

Figure 3. XRD pattern of CS and CS-Lig samples plasticised with different DES systems

CS/DESs	Characteristic peak, 2θ (°)	Crystal type
CS	15.1°, 17.2°/18.0°, 23.1°	A-type
CS–Lig–Gly	13.7° (clear peak, narrow shoulder), 19.5 and 20.1° (weak intensity), 21.2° (sharp, strong-intensity peak)	V-type
CS–Lig–C.M 1:3	13.8°, 19.1°, 21.1° (sharp, strong-intensity peak)	V-type
CS–Lig–C.G 1:3	13.6° (broad shoulder), 17.8°, 19.0°, 20.8° (sharp, strong-intensity peak)	V-type
CS–Lig–C.G.M 1:1:1	13.7°, 17.9°, 19.2°, 20.9° (sharp, strong-intensity peak)	V-type
CS–Lig–C.G.M 1:1:2	13.4° (broad shoulder), 19.2° and 19.9° (weak intensity), 21.0° (sharp, strong-intensity peak)	V-type
CS–Lig–C.G.M 1:2:1	13.7° (weak intensity), 17.4°, 19.0° and 19.8° (weak intensity), 21.1° (sharp, strong-intensity peak)	V-type

XRD pattern shows that in natural CS, characteristic peaks of A-type appear at 15.1°, 17.2/18.0°, 23.1°, representing the typical crystal type of cereal starch [21]. In the control sample (CS–Lig–Gly) and DES systems (CS–Lig–C.M 1:3; CS–Lig–C.G 1:3; CS–

Lig–C.G.M 1:1:1; 1:1:2; 1:2:1): V-type signals are simultaneously expressed at 13.4–13.8° (at different peak widths and intensities) and peaks at 20.8–21.2° (sharp/strong peaks), accompanied by weak intensity peaks at around 17.4–19.9°. The intensity and width of the peak in the 13–14° region vary depending on the composition of the DES. MEA-rich systems or ternary DES systems tend to be clearer, sharper and more ordered than Gly-rich systems.

Mechanically, DES systems, especially those containing MEA, tend to form multi-point H-bond networks with the –OH groups of starch and OH-phenolic groups of lignin, reducing the free plasticiser fraction and stabilizing the Vh-amylose single-helical complex, so the ≈ 21° peak is sharper and clearer than the Gly control sample. This XRD observation is consistent with the role of DES in both plasticisation and interphase interaction in the TPS/DES (TPS/DES) system [6, 13] and is specifically illustrated in the CS–Lig–DES system [7]. In summary, the XRD analysis data in Figure 3 reinforce that DES (especially the MEA-containing DES system) promotes more ordered V-type crystals than Gly, thereby supporting the mechanical property improvements as noted in section 3.2.

3.5. SEM images of fracture surfaces of CS-Lig samples with different plasticiser systems

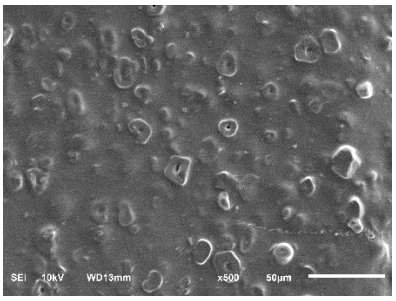

CS–Lig–Gly

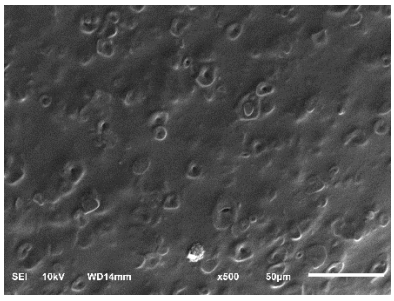

CS–Lig–C.M 1:3

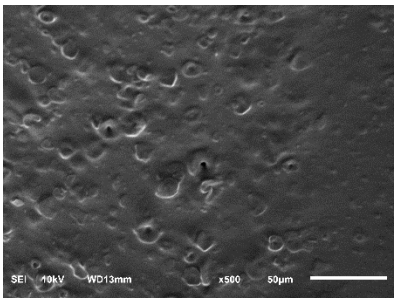

CS–Lig–C.G 1:3

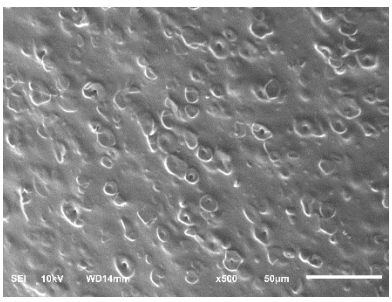

CS–Lig–C.G.M 1:1:1

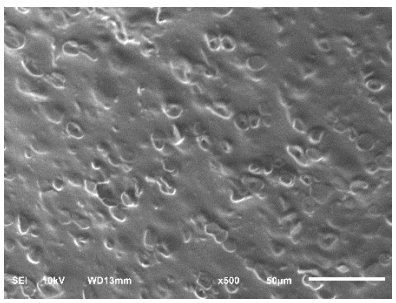

CS–Lig–C.G.M 1:1:2

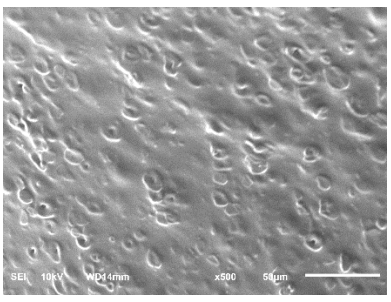

CS–Lig–C.G.M 1:2:1

Fig. 4. SEM micrographs of cryo-fractured surfaces of CS–Lig blends plasticised with Gly or DESs.

Representative cryo-fracture micrographs reveal clear, formulation-dependent differences in interfacial adhesion and deformation mechanisms. The Gly control (CS–Lig–Gly) shows relatively smooth cleavage planes interrupted by micro-voids around lignin particulates and frequent particle pull-out cavities, features of weak stress transfer and brittle failure. In contrast, DES-based formulations display progressively rougher, more tortuous fracture paths with matrix fibrillation and reduced pull-out, indicating improved interphase coupling and greater energy dissipation before failure.

Among binary DES systems, the MEA-rich CS–Lig–C.M 1:3 exhibits pronounced ductile tearing with river markings and plastic flow around embedded lignin, consistent with the concurrent gains in TS/ε_b (Table 2) and the retention upon aging (Tables 4a–b). We attribute this to dense H-bond/ion–dipole interactions between MEA (–NH/–OH) and the hydroxyl/phenolic groups of starch and lignin that suppress interfacial decohesion [6, 7, 13, 14]. The Gly-rich binary (CS–Lig–C.G 1:3) presents more matrix smearing than the control but still shows occasional debonded lignin and void coalescence, coherent with its modest TS increase and only limited ductility enhancement (Table 2).

The ternary DESs yield the most cohesive morphologies. CS–Lig–C.G.M 1:1:1 shows a markedly rough, micro-fibrillated surface and tight lignin encapsulation; CS–Lig–C.G.M 1:1:2 adds evidence of widespread plastic deformation and ligament bridging across the crack wake, microstructural signatures that accord with its high εb while maintaining a comparatively high E′ (Table 2) [7, 13, 14]. CS–Lig–C.G.M 1:2:1, which delivers the highest TS, displays crack deflection/branching and minimal particle pull-out, pointing to strong interfacial bonding and efficient stress transfer. These morphological trends dovetail with FTIR indications of intensified multi-site H-bonding (broadened, red-shifted –OH/–NH bands) and with the XRD evidence of more ordered V-type complexes—especially in MEA-containing systems, which together rationalise the simultaneous improvements in stiffness and strength [6, 7, 13, 17, 19, 20].

Notably, wettability/SFE results (Section 3.6) help nuance the picture: although the CS–Lig–C.G 1:3 surface is the most polar (higher γ^p), its fracture still reveals sporadic interfacial gaps, implying that bulk compatibilization via DES-polymer H-bond networks (reinforced by MEA) is more decisive for fracture resistance than surface polarity alone

[13]. Overall, the SEM evidence substantiates a structure–property linkage in which DES composition tunes crack-path tortuosity and interphase integrity, thereby governing the balance of strength and ductility measured mechanically.

3.6. Wettability and Surface Free Energy by Contact Angle (OWRK)

Table 3. Surface free energy components and contact angle of CS-Lig samples with Gly and DES system (mean ± SD, n = 3)

Samples	Water (θ,°)	Formamide (θ,°)	Diiodomethane (θ,°)	γ^d, mN m^{-1}	γ^p, mN m^{-1}	γ, mN m^{-1}	fp	W_{sl} mN m^{-1}	W_{12} (mN m^{-1})
CS–Lig–Gly	47.2 ± 2.8^a	43.0 ± 3.1^a	33.5 ± 2.1^a	35.9 ± 0.92	18.9 ± 1.59	54.8 ± 0.67	0.340 ± 0.02	122.25 ± 2.58	98.54 ± 0.51
CS–Lig–C.M 1:3	73.7 ± 3.1^c	60.5 ± 3.9^b	42.0 ± 3.0^b	34.2 ± 2.4	6.4 ± 1.54	40.6 ± 0.93	0.16 ± 0.03	93.29 ± 3.80	82.51 ± 0.42
CS–Lig–C.G 1:3	41.0 ± 2.9^a	39.5 ± 2.8^a	32.0 ± 2.2^a	36.1 ± 1.5	22.1 ± 1.7	58.2 ± 1.1	0.38 ± 0.02	127.70 ± 2.47	101.43 ± 0.91
CS–Lig–C.G.M 1:1:1	58.0 ± 3.4^b	48.0 ± 2.8^a	34.5 ± 1.8^a	36.7 ± 0.75	13.0 ± 1.97	49.6 ± 1.69	0.26 ± 0.03	111.33 ± 3.66	93.32 ± 1.93
CS–Lig–C.G.M 1:1:2	46.5 ± 2.9^a	43.5 ± 3.0^a	33.0 ± 1.9^a	35.9 ± 1.47	19.2 ± 1.86	55.1 ± 1.41	0.35 ± 0.02	122.87 ± 2.70	98.71 ± 1.31
CS–Lig–C.G.M 1:2:1	67.0 ± 4.8^{bc}	55.0 ± 3.9^b	36.0 ± 2.7a^b	36.4 ± 3.18	8.6 ± 2.84	45.1 ± 0.65	0.16 ± 0.05	101.18 ± 5.59	87.66 ± 0.99

Notes: W_{12} = W_{12} vs Cellulose, W_{sl} = W_{sl} (H2O)**,** Polar fraction: $f_p = \gamma^p/\gamma$. Superscripts (a, b, c) denote homogeneous groups from Tukey's HSD (α = 0.05).

Static contact angles (water, formamide, diiodomethane) were acquired on a DSA25 goniometer and surface free energy (SFE) was decomposed by the Owens–Wendt–Rabel–

Kaelble (OWRK) approach using KRÜSS ADVANCE, as described in Methods. In OWRK, SFE is partitioned into dispersive (γ^d) and polar (γ^p) components and is widely applied to polymer surfaces.

The results of Table 3 show that CS–Lig–C.G 1:3 exhibits the strongest hydrophilicity with low water angle ($\theta_{water} \approx 41°$) and the largest γ^p (≈ 22 mN m^{-1}), yielding the highest total SFE (≈ 58 mN m^{-1}). In contrast, CS–Lig–C.M 1:3 is the most hydrophobic ($\theta_{water} \approx 73.7°$) with a markedly reduced γp (≈ 6.4 mN m^{-1}) and the lowest total SFE (≈ 41 mN m^{-1}). Mixed DES systems tune surface polarity between these limits: CS–Lig–C.G.M 1:1:2 (gly-rich) is comparatively hydrophilic ($\theta_{water} \approx 46.5°$, $\gamma^p \approx 19.2$ mN m^{-1}, $\gamma \approx 55.1$ mN m^{-1}), whereas CS–Lig–C.G.M 1:2:1 shows higher θ and lower γ^p ($\theta_{water} \approx 67.0°$, $\gamma^p \approx 8.6$ mN m^{-1}, $\gamma \approx 45.1$ mN m^{-1}). Together, these data indicate θ_{water} decreases as γ^p increases, consistent with OWRK's polarity rationale.

To quantitatively connect surface-energy metrics to use-case decisions, we derived application indices from Table 3. Specifically, the polar fraction fp and the work of wetting to water W_{sl} increase with surface polarity and therefore predict improved anchorage of water-borne inks/coatings and better wetting of cellulose-rich substrates. The interfacial work of adhesion to a cellulose-like counterface, W_{12}, computed with literature OWRK components for cellulose, likewise ranks our formulations for printability/lamination (higher $W_{12} \Rightarrow$ stronger adhesion). Conversely, moisture-barrier/release tendencies can be inferred from lower W_{sl}(H2O) indicating reduced water wetting/sorption. Together, these derived indices convert the OWRK dataset into actionable formulation choices, high-γ^p systems for adhesion-critical applications vs. lower-γ^p systems for moisture resistance, without introducing new experiments. Cross-checks with DMA/SEM (strong interphase anchoring and preserved E′ for the ternary DES) support these predictions.

One-way ANOVA (Table S1) confirms between-formulation differences for all three probe liquids: Water ($F = 43.09$, $p = 2.95\times10^{-7}$), Formamide ($F = 17.93$, $p = 3.40\times10^{-5}$), and Diiodomethane ($F = 7.20$, $p = 2.5\times10^{-3}$). Tukey's HSD (Table S6-S8) pinpoints where differences occur. For water, CS–Lig–C.G 1:3 vs CS–Lig–C.M 1:3 differs by −32.63° (adjusted $p \ll 0.001$), while CS–Lig–C.G.M 1:1:1 vs CS–Lig–C.G 1:3 is also significant ($\Delta = +17.00°$, $p = 6\times10^{-4}$). For diiodomethane, CS–Lig–C.G 1:3 vs CS–Lig–C.M 1:3 remains significant ($\Delta = -10.00°$, $p = 0.0022$). The polarity trend likely reflects how plasticiser/DES chemistry mediates hydrogen-bond networks at the surface: Gly-rich

formulations expose more polar groups (higher γ^p, lower θ), whereas MEA-containing DES can immobilise polar moieties within the bulk, reducing effective surface polarity. This interpretation aligns with the established OWRK framework and contemporary reviews on DES-polymer systems that report tuneable interfacial polarity via DES composition [9, 13].

For applications requiring barrier/hydrophobic surfaces (e.g., moisture-resistant coatings), CS–Lig–C.M 1:3 or CS–Lig–C.G.M 1:2:1 are advantageous (high θ, low γ^p). Conversely, adhesion/printability may benefit from CS–Lig–C.G 1:3 or CS–Lig–C.G.M 1:1:2 (low θ, high γ^p).

3.7. Retrogradation

Table 4a. Summary of the mechanical properties of CS-Lig samples with Gly and DES system after 7, 28, and 56 days of storage (mean ± SD, n = 5)

Samples	Storage time, days							
	0		*7*		*28*		*56*	
	TS, (MPa)	*ε_b, (%)*	*TS, (MPa)*	*ε_b, (%)*	*TS, (MPa)*	*ε_b, (%)*	*TS, (MPa)*	*ε_b, (%)*
CS–Lig–Gly	1.14 ± 0.07	109.7 ± 12.3	1.13 ± 0.07	105.3 ± 11.9	1.06 ± 0.06	79.0 ± 9.6	1.01 ± 0.06	66.9 ± 8.3
CS–Lig–C.M 1:3	1.97 ± 0.14	176.9 ± 18.8	1.97 ± 0.11	173.4 ± 18.0	1.89 ± 0.12	157.4 ± 18.6	1.81 ± 0.13	143.3 ± 17.6
CS–Lig–C.G 1:3	1.36 ± 0.11	111.3 ± 13.4	1.39 ± 0.07	108.5 ± 12.0	1.28 ± 0.07	97.9 ± 11.0	1.24 ± 0.08	89.0 ± 10.0
CS–Lig–C.G.M 1:1:1	2.34 ± 0.22	152.4 ± 14.8	2.34 ± 0.15	149.7 ± 15.3	2.29 ± 0.16	136.9 ± 14.1	2.18 ± 0.16	129.5 ± 13.7
CS–Lig–C.G.M 1:1:2	2.26 ± 0.14	184.2 ± 15.8	2.24 ± 0.11	182.2 ± 16.8	2.17 ± 0.12	171.3 ± 14.2	2.12 ± 0.13	160.3 ± 13.0
CS–Lig–C.G.M 1:2:1	2.97 ± 0.18	148.6 ± 15.3	2.91 ± 0.22	145.0 ± 15.4	2.84 ± 0.22	132.3 ± 12.4	2.76 ± 0.22	123.3 ± 13.6

Table 4b. Summary of mechanical properties and % change of CS-Lig samples with Gly and DES system stored at 0 and 56 days (mean ± SD, n = 5)

No.	Samples	Storage time, days: 0		Storage time, days: 56			
		TS (MPa)	*ε_b (%)*	*TS (MPa)*	*ε_b (%)*	*Δ TS vs 0 (%)*	*Δε_b vs 0 (%)*
1	CS–Lig–Gly	1.14 ± 0.07	109.7 ± 12.3	1.01 ± 0.06	66.9 ± 8.3	−11.0 ± 8.8	−38.3 ± 11.4
2	CS–Lig–C.M 1:3	1.97 ± 0.14	176.9 ± 18.8	1.81 ± 0.13	143.3 ± 17.6	−7.7 ± 9.6	−17.8 ± 16.6

3	CS–Lig–C.G 1:3	1.36 ± 0.11	111.3 ± 13.4	1.24 ± 0.08	89.0 ± 10.0	−8.2 ± 10.8	−19.4 ± 11.9
4	CS–Lig–C.G.M 1:1:1	2.34 ± 0.22	152.4 ± 14.8	2.18 ± 0.16	129.5 ± 13.7	−5.9 ± 14.1	−14.5 ± 11.1
5	CS–Lig–C.G.M 1:1:2	2.26 ± 0.14	184.2 ± 15.8	2.12 ± 0.13	160.3 ± 13.0	−5.7 ± 11.5	−12.7 ± 7.0
6	CS–Lig–C.G.M 1:2:1	2.97 ± 0.18	148.6 ± 15.3	2.76 ± 0.22	123.3 ± 13.6	−6.6 ± 11.7	−15.8 ± 16.5

Mechanical aging of CS–Lig blends over 56 days reveals formulation-dependent retrogradation, with ductility more sensitive than strength—consistent with recrystallisation and densification of the hydrogen-bond network in starch-rich matrices during storage [6]. From Table 4a, tensile strength (TS) shows modest declines across all groups, whereas elongation at break (ε_b) decreases more markedly. For the Gly control (CS–Lig–Gly), TS drops from 1.14 ± 0.07 to 1.01 ± 0.06 MPa by day 56 (≈ −11 %), while ε_b falls from 109.7 ± 12.3 % to 66.9 ± 8.3 % (≈ −38 %), indicating substantial loss of extensibility; in contrast, DES–plasticised samples retain both properties more effectively, particularly ternary systems [5-7].

Table 4b quantifies the end-point changes (day 56 vs day 0). Ternary DESs exhibit the smallest ε_b penalties: CS–Lig–C.G.M 1:1:2 declines by only −12.7 ± 7.0 percentage points (pp), followed by 1:1:1 (−14.5 ± 11.1 pp) and 1:2:1 (−15.8 ± 16.5 pp). Binary DESs are intermediate (CS–Lig–C.M 1:3: −17.8 ± 16.6 pp; CS–Lig–C.G 1:3: −19.4 ± 11.9 pp), whereas Gly is the least stable (−38.3 ± 11.4 pp). A similar but milder ordering holds for TS: −5.7 ± 11.5 % (CS–Lig–C.G.M 1:1:2), −5.9 ± 14.1 % (CS–Lig–C.G.M 1:1:1), −6.6 ± 11.7 % (CS–Lig–C.G.M 1:2:1), −7.7 ± 9.6 % (CS–Lig–C.M 1:3), −8.2 ± 10.8 % (CS–Lig–C.G 1:3), and −11.0 ± 8.8 % (Gly). Expressed as retention at day 56, TS remains ≈ 94–93 % for ternary DESs versus 89 % for Gly; ε_b retention is ≈ 87–83 % for ternary DESs versus 61 % for Gly. The ranking underscores that ternary DESs most effectively suppress retrogradation-induced embrittlement [7, 22].

Statistically, Table 4a indicates minor changes by day 7 followed by larger decrements by days 28 and 56, especially for ε_b, supporting a robust main effect of time, with effect magnitude modulated by plasticiser composition (formulation effect). Mechanistically, the mitigation in ternary DESs is consistent with multi-site hydrogen-bond/ion–dipole interactions (e.g., ChCl-MEA-polyol) that restrain post-processing

reorganisation while preserving sufficient segmental mobility [6, 8]; by comparison, Gly-only systems provide higher free volume but are more vulnerable to subsequent stiffening and loss of extensibility during storage [3]. Overall, carefully tuned ChCl:Gly:MEA compositions (notably 1:1:2 and 1:1:1) provide a practical route to curb retrogradation over 56 days, preserving strength and limiting ductility loss relative to Gly and binary DES baselines, an advantage for applications requiring durable toughness during shelf-life [22].

In this study we adopt functional durability, the retention of tensile properties at 7/28/56 days under 23°C/50% RH—as a proxy for time-dependent microstructural evolution (retrogradation) in TPS-based matrices. In TPS, embrittlement and loss of ε_b are direct macroscopic consequences of crystallite thickening and chain re-ordering. The high retention of TS and ε_b observed for selected DES compositions therefore indicates suppressed retrogradation kinetics. This interpretation coheres with our baseline microstructural signatures: (i) the OH/NH envelope in FTIR shows low-frequency growth and broadening consistent with denser, multi-site hydrogen-bond networks, (ii) V-type features in XRD are reinforced at t = 0, and (iii) the DMA tan δ/E′ line shapes point to a broader distribution of segmental dynamics. Together these observations rationalise the mechanical stability over time without requiring additional XRD after storage. A full time-resolved structural series is outlined as future work.

Our primary objective is to provide a composition–property map for binary and ternary DESs in CS–Lig; time-resolved diffraction is beyond the scope of this map-building study and will be addressed in a dedicated follow-up.

4. Conclusions

This work establishes DES composition as a robust design lever to tune interphase interactions, mechanical response, surface polarity, and aging behaviour in CS-Lig blends. Across binary and ternary ChCl:Gly:MEA formulations, DES plasticisation consistently outperformed Gly: tensile strength increased from 1.14 MPa (control) to 2.97 MPa (CS–Lig–C.G.M 1:2:1) while elongation at break rose to ~184 % (CS–Lig–C.G.M 1:1:2). One-way ANOVA confirmed significant formulation effects for both TS and ε_b ($p < 0.001$), and Tukey's HSD resolved ternary DESs as statistically superior to the control. Mechanistically, FTIR (broadened/red-shifted –OH/–NH) and XRD (reinforced V-type ordering) corroborate denser, multisite H-bond networks in MEA-containing systems; SEM fracture surfaces transition from smooth cleavage with lignin pull-out (Gly) to

tortuous, fibrillated paths with tight particle encapsulation (DES), evidencing improved stress transfer. Surface free energy was simultaneously tuneable ($\gamma \approx 41–58$ mN m^{-1}), enabling application-specific polarity.

Aging studies (0-56-day, 23°C/50% RH) showed DES formulations mitigate retrogradation-induced embrittlement: ternary systems retained ~93–94 % TS and ~83–87 % ε_b versus ~89 % and ~61 % for Gly, respectively. In practice, CS–Lig–C.G.M 1:2:1 is recommended where strength and stiffness dominate, whereas CS–Lig–C.G.M 1:1:2 is preferred when ductility and toughness are prioritised, both delivering superior stability over time. These findings advance bio-based CS-Lig plastics toward more durable, property-balanced materials and provide clear, composition-property maps for process selection. Future work should examine DES migration and long-term hydrothermal aging, moisture/barrier trade-offs under variable humidity, recyclability, and end-of-life biodegradation under relevant standards, alongside scale-up via continuous twin-screw processing and LCA to quantify sustainability benefits.

Phuong Thi Hoang, Chien Nguyen Van, Phuong Ha Doan, Trang Quynh Pham

CRediT author statement

Phuong Thi Hoang: Supervision, Reviewing and Editing, Chien Van Nguyen, Mai Thi Pham: Conceptualisation, Literature Review, Data Analysis, Writing - Original Draft Preparation; Chien Van Nguyen, Phuong Ha Doan, Trang Quynh Pham: Conceptualisation, Literature Review, Data Analysis, Writing - Original Draft Preparation.

ACKNOWLEDGEMENTS

The current research received funding from the Vietnam Academy of Science and Technology under grant number TĐNSH0.4/22-24.

COMPETING INTEREST

The authors declare that there is no conflict of interest regarding the publication of this article.

REFERENCES

[1] Diaz-Baca, J.A. and P. Fatehi (2024), "Production and characterisation of starch-lignin based materials: A review". *Biotechnology Advances*. **70**: p. 108281.

[2] Surendren, A., et al. (2022), "A review of biodegradable thermoplastic starches, their blends and composites: recent developments and opportunities for single-use plastic packaging alternatives". *Green Chemistry*. **24**(22): p. 8606-8636.

[3] Lai, D.S., et al. (2022), "Effective aging inhibition of the thermoplastic corn starch films through the use of green hybrid filler". *Polymers*. **14**(13): p. 2567.

[4] Eslami, Z., et al. (2023), "A review of the effect of plasticisers on the physical and mechanical properties of alginate-based films". *Molecules*. **28**(18): p. 6637.

[5] Zdanowicz, M. and K. Sałasińska (2023), "Characterisation of thermoplastic starch plasticised with ternary urea-polyols deep eutectic solvent with two selected fillers: microcrystalline cellulose and montmorillonite". *Polymers*. **15**(4): p. 972.

[6] Skowrońska, D. and K. Wilpiszewska (2022), "Deep eutectic solvents for starch treatment". *Polymers*. **14**(2): p. 220.

[7] Zdanowicz, M., et al. (2022), "Thermoplastic starch/ternary deep eutectic solvent/lignin materials: study of physicochemical properties and fire behaviour". *ACS Sustainable Chemistry & Engineering*. **10**(14): p. 4579-4587.

[8] Wang, H., et al. (2019), "Insights into the hydrogen bond interactions in deep eutectic solvents composed of choline chloride and polyols". *ACS Sustainable Chemistry & Engineering*. **7**(8): p. 7760-7767.

[9] Owens, D.K. and R. Wendt (1969), "Estimation of the surface free energy of polymers". *Journal of applied polymer science*. **13**(8): p. 1741-1747.

[10] Cwikel, D., et al. (2010), "Comparing contact angle measurements and surface tension assessments of solid surfaces". *Langmuir*. **26**(19): p. 15289-15294.

[11] Hubbe, M.A. and D.J. Gardner (2015), "Contact angles and wettability of cellulosic surfaces: a review of proposed mechanisms and test strategies". *BioResources*. **10**(4).

[12] Saito, T., et al. (2014), "Methanol Fractionation of Softwood Kraft Lignin: Impact on the Lignin Properties". *Chem. Sus. Chem.* **7**(1): p. 221-228.

[13] Weerasinghe, U.A., et al. (2024), "Deep eutectic solvents towards green polymeric materials". *Green Chemistry*. **26**(15): p. 8497-8527.

[14] Mascia, L., et al. (2020), "Antiplasticization of polymer materials: Structural aspects and effects on mechanical and diffusion-controlled properties". *Polymers*. **12**(4): p. 769.

[15] Mojica-Muñoz, D.M., et al. (2024), "Optimizing biodegradable plastics: Molecular dynamics insights into starch plasticisation with glycerol and oleic acid". *Journal of Molecular Graphics and Modelling*. **126**: p. 108674.

[16] Linan, L.Z., et al. (2024), "Benefits of incorporating lignin into starch-based films: a brief review". *Polymers*. **16**(16): p. 2285.

[17] Sun, X., et al. (2023), "Sustainable starch/lignin nanoparticle composites biofilms for food packaging applications". *Polymers*. **15**(8): p. 1959.

[18] Eugenio, M.E., et al. (2021), "Properties versus application requirements of solubilised lignins from an elm clone during different pre-treatments". *International journal of biological macromolecules*. **181**: p. 99-111.

[19] Chen, H., et al. (2023), "Study on the solubility of industrial lignin in choline chloride-based deep eutectic solvents". *Sustainability*. **15**(9): p. 7118.

[20] Xia, Q., et al. (2018), "Multiple hydrogen bond coordination in three-constituent deep eutectic solvents enhances lignin fractionation from biomass". *Green chemistry*. **20**(12): p. 2711-2721.

[21] Zhou, Q., et al. (2025), "V-type granular starches derived from different starch varieties: an exploration of the relationships between structure, physicochemical properties, and emulsifiability: Q. Zhou et al". *Food Science and Biotechnology*: p. 1-15.

[22] Zdanowicz, M. and C. Johansson (2016), "Mechanical and barrier properties of starch-based films plasticised with two-or three component deep eutectic solvents". *Carbohydrate Polymers*. **151**: p. 103-112.